TGF-β1 signaling remodels T_H17 cell chromatin architecture for metabolic reprogramming

Authors

Xiang Yu[1, *], Li Wang[1, *], Chao Yao[2], Rong Qiu[2], Yange Cui[2], Dai Dai[3], Jun Deng[3], Guojun Hou[2], Yan Wang[2], Jie Qian[1], Ye Ouyang[1], Yuting Qin[3], Bo Qu[1], Haibo Zhou[3], Youcun Qian[2], Yuanjia Tang[1], Nan Shen[1,2,3,4]

Affiliations

[1] Shanghai Institute of Rheumatology, Renji Hospital, Shanghai Jiao Tong University School of Medicine, Shanghai, China.
[2] Institute of Health Sciences, Shanghai Jiao Tong University School of Medicine and Shanghai Institutes for Biological Sciences (SIBS), University of Chinese Academy of Sciences, Chinese Academy of Sciences (CAS), Shanghai, China.
[3] China-Australia Centre for Personalized Immunology, Renji Hospital, Shanghai Jiao Tong University School of Medicine, Shanghai, China.
[4] Center for Autoimmune Genomics and Etiology (CAGE), Cincinnati Children's Hospital Medical Center, Cincinnati, Ohio, USA.
Correspondence to Nan Shen, MD, Department of Rheumatology, Renji Hospital, Shanghai Jiao Tong University School of Medicine, 145 Shan Dong Road (c), Shanghai 200001, China. E-mail: nanshensibs@gmail.com.
* These authors contributed equally.

Summary

T_H17 cells exhibit great heterogeneity and variable functional states in vivo. However, metabolic reprogramming of T_H17 cells in vivo and its regulation during autoimmunity and host defence is unknown. Here we report that T_H17 cells derived in vivo show discrete metabolic states. Metabolic states of T_H17 cells in vivo were controlled at the epigenetic level, with conserved regulatory region of key metabolic regulators show distinct chromatin accessibility as

demonstrated by chromatin landscape profiling. TGF-β1 signaling was further shown to be crucial for remodeling of T_H17 cell chromatin states, *Ahr* and *miR-21* were identified as essential metabolic regulators for T_H17 cells. Understanding metabolic reprogramming of T_H17 cells in vivo may therefore provide more defined therapeutic intervention to T_H17 cell mediated autoimmune diseases and insights into T_H17 cell mediated host defence.

Keywords

T_H17 cell, metabolic reprogramming, chromatin states, microRNAs

Introduction

T_H17 cells, which have been characterized as a subset of effector $CD4^+$ helper T cells that produce IL-17A(Littman and Rudensky, 2010), mediate barrier tissue integrity, mucosal defence, and also contribute to the development of multiple autoimmune diseases. At steady state condition, T_H17 cells producing IL-10 are mainly found at sites of intestinal lamina propria (Ivanov et al., 2009; Sano et al., 2015). Under autoimmune or pathogen infection condition, T_H17 cells acquire the capability to produce IFNγ or GM-CSF, and are often seen at sites of inflamed loci(Atarashi et al., 2015; Stockinger and Omenetti, 2017). T_H17 cells also could be differentiated in vitro by a combination of cytokines TGF-β1, IL-6 or IL-6, IL-1β and IL-23(Gaublomme et al., 2015; Ghoreschi et al., 2010).

Upon antigen stimulation, lymphocytes undergo extensive clonal expansion and differentiation for immune defense or tolerance(Boothby and Rickert, 2017;

Buck et al., 2015; Man and Kallies, 2015; Pollizzi and Powell, 2014). Activated lymphocytes are highly metabolic and demonstrate a striking increase in cell content and nutrients uptake. c-Myc, Hif1a, c-Rel and mTORc1-dependent metabolic activity is crucial for effective T and B cell immune response(Heise et al., 2014; Shi et al., 2011; Verbist et al., 2016; Wang et al., 2011), whereas Foxo1 and Foxp3 proteins function as key metabolic repressors that contain glycolytic activity in Treg cells(Angelin et al., 2017; Cho et al., 2016; Wilhelm et al., 2016). Recently it is reported that by restricting glucose availability, tumor cells limit aerobic glycolysis and effector function of tumor-infiltrating T cells(Chang et al., 2015; Ho et al., 2015). However, metabolic states of T_H17 cells in vivo under different circumstances is incompletely understood, and how T_H17 cells adapt to microenvironment with distinct nutrients supply is not known.

Recently, tight communication between epigenetic remodeling and metabolic reprogramming for immune cell plasticity is beginning to be understood(Etchegaray and Mostoslavsky, 2016; Kinnaird et al., 2016), substrates and cofactors of many epigenetic modifying enzymes are indeed intermediates of specific metabolic pathways(Xu et al., 2017). Assay for transposase-accessible chromatin (ATAC-seq) technology was developed to study global chromatin dynamics by using relatively low cell number(Buenrostro et al., 2013). It was successfully used to study chromatin dynamics of Treg cells under inflammatory condition(van der Veeken et al., 2016), the development of plasmacytoid DC (Ceribelli et al., 2016) and tumor-specific $CD8^+$ T cells(Philip

et al., 2017). However, chromatin states of T_H17 cells in vivo and their regulation of T_H17 cell metabolic reprogramming is unknown. Signaling pathways which are essential for T_H17 cell chromatin remodeling in vivo are also incompletely understood.

MicroRNAs are a class of noncoding RNAs that modulate gene expression at the posttranscriptional level(Mehta and Baltimore, 2016). Specific microRNAs have been reported to be essential for the metabolic function of certain cells, such as *miR-33a/b* was shown to be crucial for cholesterol and lipid metabolism(Najafi-Shoushtari et al., 2010; Rayner et al., 2010) and let-7 family members were recently shown to be essential for B cell metabolic function(Jiang et al., 2018; Zhu et al., 2011). The regulation of T_H17 cell metabolic reprogramming in vivo by microRNAs is not well understood.

In this study, first by metabolomics study we found in vitro derived T_H17 cells under non-pathogenic and pathogenic condition had distinct metabolic states. Further by RNA-seq of T_H17 cells derived in vivo under homeostatic and autoimmune condition, we demonstrate that T_H17 cells adapt to microenvironment with discrete metabolic states. And the metabolic states of T_H17 cells in vivo was regulated at the epigenetic level as revealed by chromatin landscape profiling. TGF-β1 signaling was further shown to be crucial for remodeling of T_H17 cell chromatin states, *Ahr* and *miR-21* were identified as essential regulators for T_H17 cell metabolic reprogramming.

Results

T_H17 Cells derived in vitro show discrete metabolic states

To study the metabolic activity of T_H17 cells, first we induced T_H17 cells in vitro by a combination of cytokines TGF-β1, IL-6 (T_H17 (b)) or IL-6, IL-1β and IL-23 (T_H17 (23)). Interestingly, we consistently observed that T_H17 (23) cells show increased cell size compared to T_H17 (b) cells (Figure S1A-B), which indicate that T_H17 (23) cells are more metabolically activated. We further tested the metabolic potential of T_H17 (b) and T_H17 (23) cells by analyzing key metabolic regulators and enzymes, we found p-S6 and HKII were immediately activated during T_H17 cell differentiation, and T_H17 (23) cells were much more glycolytic than T_H17 (b) cells, T_H17 (23) cells express great more p-S6, HKII at the protein level (Figure 1A). To study early metabolic requirements needed for T_H17 cell differentiation, we checked key metabolic activators and repressors at an earlier time point, 30h after initial activation, we found T_H17 (23) cells express great more HKII, Glut1, p-S6 and c-Myc, while express lower level of the metabolic repressor protein Foxo1 (Figure 1B-C). To study the metabolic potential of T_H17 cells more clearly, we sorted GFP^+ T_H17 cells differentiated in vitro from IL17A-eGFP reporter mice, again we found T_H17 (23) cells express great more HKII, the rate limiting enzyme for glycolysis (Figure 1D).

We further subjected T_H17 (b) and T_H17 (23) cells for high-resolution metabolomics analyses(Chen et al., 2014; Chen et al., 2016). Pathogenic T_H17 (23) cells were metabolically distinct from T_H17 (b) cells (Figure 1E, Figure S1C),

and showed higher level intermediates of carbohydrates, amino acids and organic acids, while T_H17 (b) cells showed higher level intermediates of nucleotides and fatty acids. Pathway analyses of altered metabolites showed that amino acid, amino sugar metabolism, and glycolytic intermediates trended to be higher in T_H17 (23) cells (Figure 1F, Table S1). Taken together, these data suggest that T_H17 cells differentiated in vitro under non-pathogenic and pathogenic condition have distinct metabolic states.

T_H17 Cells in vivo show discrete metabolic states

To gain insight of the metabolic reprogramming of T_H17 cells in vivo, we immunized IL17A-eGFP mice with MOG_{35-55} emulsified in complete adjuvant to induce autoimmune encephalomyelitis (EAE), and infected IL17A-eGFP mice with enteric pathogen *Citrobacter Rodentium* to induce colitis. Then we isolated and sorted GFP^+ T_H17 cells from homeostatic ileum, CNS of EAE mice at the peak of disease and *Citrobacter*-infected colon tissue (Figure S2A). Interestingly after gating on GFP^+ T_H17 cells, we found CNS-infiltrated and *Citrobacter*-induced T_H17 cells had significantly increased cell size compared to ileum homeostatic T_H17 cells (Figure 2A), which indicate T_H17 cells derived under autoimmune and pathogen infection condition are more metabolically activated. To gain a more global view of functional and metabolic states of T_H17 cells in vivo, we sent ileum homeostatic and CNS-infiltrated T_H17 cells for RNA-seq analyses. We found 1415 upregulated genes and 1249 downregulated genes in CNS-infiltrated T_H17 cells compared to ileum homeostatic T_H17 cells

(Figure S2B-C). GO and Pathway analyses indicate that several immune pathways were activated in CNS-infiltrated T_H17 cells as reported(Gaublomme et al., 2015), interestingly, we found multiple metabolic pathways were enriched (Figure 2B), of the 1415 upregulated genes, almost 10% were involved in metabolic process, which indicate T_H17 cells adapt to diverse microenvironment with discrete metabolic states. We also found homeostatic ileum T_H17 cells express great more *Foxp1 gene* (Figure 2C), which is critical for maintenance of the metabolic quiescence of naive T cells(Feng et al., 2011; Stephen et al., 2014), suggest it would play a similar role here by keep the quiescence of ileum homeostatic T_H17 cells. Ileum homeostatic T_H17 cells also express several transcription factors with repressor activity *c-Maf* and *Foxo1*, and Foxo1 was a repressor of glucose metabolism(Wilhelm et al., 2016) (Figure 2C), which is consistent with our finding that CNS-infiltrated T_H17 cells express higher level genes of the glucose metabolism pathway (Figure 2D). Further analyses of the data revealed that of the 66 differentially expressed solute carrier family genes, almost 70% were upregulated in CNS-infiltrated T_H17 cells (Figure 2E), which indicate that T_H17 cells in vivo adapt to microenvironment with distinct pattern of solute carrier proteins for different nutrients availability. Taken together, these data suggest that T_H17 cells in vivo adapt to microenvironment with discrete metabolic states to facilitate their inflammatory or regulatory function.

Chromatin states define T_H17 Cell metabolic reprogramming in vivo

To dissect possible regulation mechanism for T_H17 cell metabolic reprogramming in vivo, we performed ATAC-seq to assess chromatin landscape genome-wide of T_H17 cells derived in vivo. We found that T_H17 cells had discrete chromatin states in vivo (Figure 3A-B), CNS infiltrating T_H17 cells showed great differential global chromatin accessibility compared to ileum homeostatic T_H17 cells. Principle component analysis of enriched peaks indicated that T_H17 cells in vivo had discrete chromatin states (Figure 3C), with the major variance came from CNS infiltrating T_H17 cells, chromatin states of ileum homeostatic and *Citro Rodentium* induced colon T_H17 cells were much similar, which indicate these two types of T_H17 cells may have similar functional property, for mucosal defense against intestinal pathogens. Interestingly, the regulatory region of key T_H17 cell-related transcription factors c-*Maf* and *Ahr* was with reduced chromatin accessibility in CNS infiltrating T_H17 cells, both c-Maf and Ahr were shown to be critical regulators of T_H17 cells. The regulatory region of metabolic repressor Foxo1 was with reduced chromatin accessibility in CNS-infiltrated T_H17 cells, which suggests that CNS-infiltrated T_H17 cells were relieved from Foxo1-mediated metabolic repression (Figure 3D). A group of genes related to metabolic pathways and solute carrier family members were also with enhanced chromatin accessibility in CNS-infiltrated T_H17 cells, which was consistent with the gene expression data (Figure 3D, Figure S3). Taken together, these data suggest that metabolic reprogramming of T_H17 cells in vivo were controlled at the epigenetic level.

TGF-β1 signaling remodels T_H17 cell chromatin architecture for metabolic reprogramming

To define the regulation mechanism for T_H17 cell chromatin remodeling, we differentiated T_H17 cells in vitro either in the presence (T_H17 (b)) or absence (T_H17 (23)) of TGF-β1 signaling and sorted out GFP^+ T_H17 cells. Then we performed ATAC-seq to assess chromatin landscape genome-wide of T_H17 cells derived in vitro. We found T_H17 cells derived in vitro had discrete chromatin states (Figure 4A), T_H17 (23) cells showed great differential global chromatin accessibility compared to T_H17 (b) cells by principle component analysis of enriched peaks (Figure 4B). Interestingly, the regulatory region of key metabolic regulators c-Myc and c-Rel was with decreased chromatin accessibility in T_H17 cells derived in the presence of TGF-β1 signaling (Figure 4C), which is consistent with the reports that TGF-β1 signaling represses c-Rel-dependent c-Myc expression during lymphocytes activation(Arsura et al., 1996; Grumont et al., 2004), and suggests that TGF-β1 signaling mediates chromatin remodeling of key metabolic regulators for metabolic reprogramming in vivo.

The regulatory region of key T_H17 cell-related transcription factors c-*Maf* and *Ahr* was with increased chromatin accessibility in T_H17 cells derived in the presence of TGF-β1 signaling (Figure 4C), which is consistent with the reports that TGF-β1 signaling induces Ahr and c-Maf expression(Gagliani et al., 2015; Ghoreschi et al., 2010). To check out whether Ahr signaling was required for T_H17 cell metabolic reprogramming in vivo, we differentiated T_H17 cells in vitro

either in the presence of Ahr agonist FICZ or antagonist CH-223191, we found that Ahr agonist efficiently decreased p-S6 protein level while upregulated the metabolic repressor Foxo1 protein, whereas Ahr antagonist significantly increased p-S6 level of T_H17 cells while downregulated Foxo1 protein (Figure S4), these data suggest that TGF-β1 signaling-dependent Ahr promotes metabolic quiescence of T_H17 cells at mucosal surfaces under steady-state condition. A group of genes related to metabolic pathways and solute carrier family members were also with decreased chromatin accessibility in T_H17 cells derived in the presence of TGF-β1 signaling, which was also consistent with their relative protein expression level (Figure 4D, Figure 1A-D). Taken together, these data suggest that TGF-β1 signaling remodels T_H17 cell chromatin states for metabolic reprogramming.

MiR-21 regulates metabolic reprogramming of T_H17 cells through Peli1-c-Rel axis

Specific microRNAs are appreciated as key metabolic regulators for immune cell function, interestingly, we found that the regulatory region of certain microRNAs showed great more chromatin accessibility in CNS infiltrating T_H17 cells compared to ileum homeostatic T_H17 cells, which include *miR-21, miR-23a cluster,* and *miR-210* (Figure 5A). The regulatory region of *miR-125a* cluster was with reduced chromatin accessibility in CNS infiltrating T_H17 cells, which indicate that this microRNA cluster might have some regulatory role in homeostatic T_H17 cells, as reported for its regulatory role in regulatory T

cells(Pan et al., 2015). The regulatory region of *miR-155, miR-146, miR-17-92 cluster* and *miR-183-96-182* cluster was with equivalent chromatin accessibility between T_H17 cells derived at different conditions in vivo (Figure S5A).

Our group previously demonstrated that miR-21 was highly upregulated in inflammatory lesions of multiple human autoimmune diseases(Zhu et al., 2012). To better understand the general functional features of miR-21-deficient T_H17 cells, we differentiated naïve T cells from control and *miR-21*$^{-/-}$ mice in vitro under pathogenic T_H17-skewing condition, RNA was extracted and subjected to RNA-seq. We then analyzed the gene list for enrichment of gene ontology and canonical pathways using the DAVID bioinformatics databases(Huang da et al., 2009). In the absence of miR-21, T_H17 cells showed decreased expression of T_H17 cell signature genes, which include lineage-specific transcription factors, cytokines, and cytokine receptors (Figure 5B). Remarkably, many of the genes involved in glycolytic or related metabolic pathways were highly enriched, include key transporters for glucose intake, *Slc2a1/3*, and rate-limiting enzymes, *Hk1/2*, *Pfkl*, *Pgm2*, *Ldha* and *Pdk1* (Figure 5B, Figure S5B). We further checked the glycolytic activity of control and *miR-21*$^{-/-}$ T_H17 cells by glycolysis stress test for extracellular acidification rate, both basal and maximal glycolytic capability were greatly decreased in *miR-21*$^{-/-}$ T_H17 cells (Figure 5C). By sorting out GFP^{+} control and *miR-21*$^{-/-}$ T_H17 cells differentiated from IL17A-eGFP mice, we found *miR-21*$^{-/-}$ T_H17 (23) cells show significant lower p-S6 protein level compared to control T_H17 (23) cells (Figure 5D), which indicates

that miR-21 is indeed critical for metabolic reprogramming of T_H17 cells.

To further investigate the precise mechanism underlying miR-21 promotes T_H17 cell metabolic reprogramming, we screened the direct targets of miR-21 by combining target prediction with Ago2 HITS-CLIP(Loeb et al., 2012), TargetScan and RNA-seq data to identify overlapping gene transcripts. Using a combination of these three approaches, we identified 5 common putative targets (*Esyt2, Mbnl1, Pdcd4, Peli1,* and *Psrc1*) (Figure 5E). Among them, *Peli1* has been reported to function as a negative regulator of $CD4^+$ T cell activation by ubiquitination of c-Rel and *Peli1*$^{-/-}$ mice spontaneously developed autoimmune disease(Chang et al., 2011). c-Rel was reported to induce *c-Myc* expression in activated T cells(Arsura et al., 1996; Grumont et al., 2004), and was a metabolic regulator of germinal center B cell function(Heise et al., 2014), therefore we chose *Peli1* for further analysis (Figure 5F). By in vitro RNA immunoprecipitation assay, we found Ago2-immunoprecipitated RNAs had significantly reduced Peli1 mRNA level in *miR-21*$^{-/-}$ T_H17 (23) cells (Figure 5G), which suggests that Peli1 is a functional target of miR-21 in T_H17 cells. We further validated these at the protein level in purified GFP^+ T_H17 cells differentiated in vitro, we found that *miR-21*$^{-/-}$ T_H17 cells have elevated level of Peli1 protein, whereas the protein level of c-Rel was reduced in *miR-21*$^{-/-}$ T_H17 cells (Figure 5H). Interestingly, we found that T_H17 (23) cells expressed substantially high level of c-Rel compared to T_H17 (b) cells, and TGFβ1 signaling is required for the repression of c-Rel expression (Figure S5C). Taken

together, these data suggest that miR-21 targets the *Peli1*-c-Rel pathway to promote metabolic reprogramming of pathogenic T_H17 cells.

MiR-21 regulates T_H17 cells during autoimmunity and mucosal defence

To determine the role of miR-21 in a T_H17 cell dominant disease model, we performed passive EAE to specifically address the role of miR-21 in mediating CNS inflammation induced by pre-activated $MOG_{35–55}$-specific T_H17 cells (Figure S6A-C). When adoptively transferred into naive recipient mice, only control MOG-specific T_H17 cells efficiently induced EAE (Figure S6D), *miR-21*$^{-/-}$ T_H17 cells failed to induce EAE, emphasizing an indispensable role of miR-21 in mediating the cell-intrinsic effector function of T_H17 cells.

To exclude any possible role of miR-21 in dendritic cells and other myeloid cells that could contribute to EAE disease pathogenesis, we bred *miR-21*$^{f/+}$ allele to CD11c-cre and Lyz-cre, to delete miR-21 in dendritic cells, neutrophils, macrophages and microglia (Figure. S6E-F). Loss of miR-21 expression in dendritic cell and myeloid cell compartment did not protect mice from autoantigen challenge (Figure 6A). When immunized with MOG_{35-55} in CFA, CD4-cre *miR-21*$^{f/f}$ mice were highly resistant to EAE compared to littermate CD4-cre mice (Figure 6B-E). At the peak of disease, CD4-cre *miR-21*$^{f/f}$ mice had less infiltrating of $CD4^+$ IL-17A$^+$ IFNγ$^+$ and IL17A$^+$ GM-CSF$^+$ T_H17 cells.

To explore miR-21 mediated T_H17 cell function in an enteric pathogen infection condition, we used *Citrobacter Rodentium*-induced colitis, mice-deficient of Il17A gene exhibit much severe colitis and bacteria clearance(Basu et al., 2015).

After gavage control and CD4-cre *miR-21*$^{f/f}$ mice with *Citrobacter*, we found that CD4-cre *miR-21*$^{f/f}$ mice suffered from more severe colitis, with significantly shorter colon and increased luminal bacteria load by day 14 compared to control mice (Figure 6F-G). Further analyses of colon lamina propria lymphocytes revealed that infected CD4-cre *miR-21*$^{f/f}$ mice had significantly lower number of total CD4^{+} T cells, T_H17 and T_H1 cells, albeit with the same number of T_H17*1 cells (Figure 6H-K). Taken together, these data demonstrate that miR-21 mediates autoimmune disease and mucosal defence through T_H17 cells in a CD4^{+} T cell intrinsic manner.

Discussion

T_H17 cells exhibit great heterogeneity in vivo, the basic energy requirement of T_H17 cells for their regulatory or inflammatory function under homeostatic or autoimmune and pathogen infection condition was not examined. And how T_H17 cells adapt to diverse tissue microenvironment with distinct nutrients availability and regulation of their metabolic reprogramming in vivo were not known.

In the present study, by metabolomics analyses of in vitro derived T_H17 cells, we found that T_H17 cells respond to different stimulations with distinct metabolic activity. And by global transcriptome analyses of in vivo derived T_H17 cells, we first showed T_H17 cells adapt to tissue microenvironment with discrete metabolic states in vivo.

To dissect the regulation of T_H17 cell metabolic states in vivo, we performed

genome-wide chromatin landscape profiling and found that T_H17 cells had discrete chromatin states in vivo. The regulatory region of key T_H17 cell-related transcription factors, metabolic regulators, metabolism-related genes and microRNAs were with differential chromatin accessibility between homeostatic ileum T_H17 cells and CNS infiltrating T_H17 cells. Interestingly, colon T_H17 cells from *Citro Rodentium* infected mice had similar chromatin status with homeostatic ileum T_H17 cells, which indicates that they have similar anti-bacteria function in vivo. Our data suggests that T_H17 cells in vivo adapt to distinct microenvironment with discrete epigenetic and metabolic states, and metabolic regulators and metabolism-related genes were regulated at the epigenetic level for their functional requirements. TGF-β1 signaling was further shown to be crucial for remodeling of T_H17 cell chromatin states in vitro, *Ahr* was identified as essential metabolic regulators for T_H17 cells.

Interestingly, we found the conserved regulatory region of a group of small microRNAs were with differential chromatin accessibility of T_H17 cells derived in vivo, which could have contributed to the regulation of discrete metabolic states of T_H17 cells in vivo for the fine-tune property of microRNAs. The regulatory region of miR-21 was with increased chromatin accessibility in CNS infiltrating T_H17 cells. Although miR-21 was shown previously to be important in T_H17 cell generation(Murugaiyan et al., 2015), its exact action has not been well understood. By global transcriptomics analyses, we demonstrate that miR-$21^{-/-}$ T_H17 cells express less T_H17 cell signature genes and key metabolism

pathway genes. Further by purify T_H17 cells differentiated from IL17A-eGFP mice, we found *miR-21*$^{-/-}$ T_H17 cells had reduced mTORc1 activity, with dramatically reduced intracellular p-S6 level. These data suggest that with increased chromatin openness of its regulatory region, miR-21 regulates metabolic reprogramming of T_H17 cells under autoimmune inflammation.

To survey for putative targets of miR-21 in pathogenic T_H17 cells, we combined target prediction with previously reported miR-21 Ago HITS-CLIP data, TargetScan and our RNA-seq data to identify overlapping gene transcripts. Using a combination of these three approaches, we identified Peli1 as a functional target of miR-21 in pathogenic T_H17 cells. Peli1 has been reported to function as a negative regulator of $CD4^+$ T cell activation by ubiquitination of c-Rel and *Peli1*$^{-/-}$ mice spontaneously developed autoimmune disease. To our knowledge, our study identifies the first evidence that by targeting key downstream regulators of TCR signaling miR-21 promotes the metabolic reprogramming of T_H17 cells and regulates T_H17 cell during autoimmunity and host defence.

T_H17 cells mediate pathogenic role in multiple autoimmune diseases. Though anti-IL-17A treatment received great efficacy in psoriasis, it badly failed for IBD patients. Understanding metabolic reprogramming of T_H17 cells in vivo may therefore provide more defined therapeutic intervention to T_H17 cell mediated autoimmune diseases and insights into T_H17 cell mediated host defence. The microenvironment of homeostatic mucosal surfaces and various inflammatory

sites could have great differential effects on chromatin states of T_H17 cells in vivo, which in turn could facilitate their discrete metabolic reprogramming. Our study so far dissected the metabolic states and chromatin states of T_H17 cells in vivo and identified *miR-21* as a critical metabolic regulator of pathogenic T_H17 cells.

Methods

Mice

MiR-21$^{-/-}$ and *miR-21* $^{f/+}$ mice on the C57B6 background were from Biomodel Organism (Shanghai, China). CD4-cre, Lyz-cre, CD11c-cre and *Stat3* $^{f/+}$ mice were from Jackson lab. IL17A-eGFP reporter mice were from Biocytogen. All mice were maintained under specific pathogen-free conditions. All animal experiments were performed in compliance with the guide for the care and use of laboratory animals and were approved by the institutional biomedical research ethics committee of the Shanghai Institutes for Biological Sciences (Chinese Academy of Sciences).

Cell culture

Naïve $CD4^+$ T cells were isolated from lymph nodes or spleen of mice using a $CD4^+$ $CD62L^+$ T cell isolation kit II (Miltenyi Biotec) according to the manufacturer's instruction. Naïve $CD4^+$ T cells were stimulated with plate-bound anti-CD3ε mAb (5 μg/ml) in the presence of anti-CD28 mAb (2 μg/ml) in

a 48-well plate under neutral conditions (10 µg/ml anti–IL-4 mAb and 10 µg/ml anti–IFN-γ mAb), IL-6 conditions (10 ng/ml IL-6, 10 µg/ml anti–IL-4 mAb, and 10 µg/ml anti–IFN-γ mAb), T_H17 (b) conditions (2 ng/ml TGF-β, 20 ng/ml IL-6, 10 µg/ml anti–IL-4 mAb, and 10 µg/ml anti–IFN-γ mAb), T_H17 (23) conditions (20 ng/ml IL-6, 20 ng/ml IL-1β, 20 ng/ml IL-23, 10 µg/ml anti–IL-4 mAb, and 10 µg/ml anti–IFN-γ mAb). Ahr agonist FICZ was used at 100 nM, Ahr antagonist CH-223191 was used at 10 uM.

Antibodies and reagents

Antibodies to mouse CD3ε (145-2C11), CD28 (37.51), IL-4 (11B11), IFN-γ (XMG1.2), CD3ε PerCP5.5 (145-2C11), Foxp3 APC (FJK-16s), ROR gamma (t) PE (B2D) and GM-CSF PE (MP1-22E9) were from eBiosciences. FICZ and CH-223191 were from Sigma. Antibodies to mouse CD45 APC-cy7 (30-F11), CD4 BV510 (RM4-5), IL-17A PE (TC11-18H10), IFN-γ APC (XMG1.2) were from BD Biosciences. Recombinant Mouse IL-6, IL-1β, IL-23, and TGF-β1 protein were purchased from R&D Systems. Peli1 (F-7) was from Santa cruz, c-Rel (D4Y6M), Foxo1 (C29H4), p-S6 (2F9), c-Myc (D3N8F), HKII (C64G5) were from Cell signaling. Glut1 (EPR3915) antibody was from Abcam. RIPAb+ Ago2 was from Merk millipore. XF Glycolysis Stress Test Kit was from Agilent technologies.

Intracellular cytokine staining

Cultured or tissue isolated lymphocytes were washed and stimulated with PMA

(50 ng/ml) plus ionomycin (750 ng/ml) for 4 h at 37°C. Cells were stained with anti-CD45 APC-cy7, anti-CD3ε PerCP5.5 and anti-CD4 BV510 for 30 min at 4°C. Cells were then fixed, permeabilized with Perm/Wash buffer (BD), and stained with anti–IFN-γ APC, anti-GM-CSF PE or anti–IL-17A PE for 30 min at 4°C. Cytokine profiles of $CD4^+$ cells were analyzed on a FACSCalibur with FlowJo software (Tree Star).

Induction of EAE

IL17A-eGFP reporter mice, $CD4^{cre}$ *miR-21*$^{fl/fl}$ mice and littermate CD4-cre or *miR-21*$^{fl/fl}$ mice were injected subcutaneously in the tail base with MOG35-55 peptide (200 μg/mouse, MEVGWYRSPFSRVVHLYRNGK) in complete Freund's adjuvant. 5 min and 48 h after the injection of MOG35-55 peptide, the mice were injected intraperitoneally with pertussis toxin (200 ng/mouse; Sigma-Aldrich). Status of the mice was monitored, and disease severity was scored three times a week as follows: 0 = no clinical signs, 1 = limp tail (tail paralysis), 2 = complete loss of tail tonicity or abnormal gait, 3 = partial hind limb paralysis, 4 = complete hind limb paralysis, 5 = forelimb paralysis or moribund, 6 = death. Cells were isolated from whole brain and spinal cord at the peak of disease by Percoll gradient centrifugation (37%/70%) and subjected to flow cytometric analysis or flow cytometric sorting.

***Citro Rodentium* infection**

C. rodentium strain DBS100 (ATCC51459; American Type Culture Collection)

were prepared by shaking of bacteria overnight at 37 °C in Luria-Bertani broth. Bacterial cultures were serially diluted and plated on MacConkey agar plates so the CFU dose administered could be confirmed. For infection, IL17A-eGFP reporter mice were oral inoculated with 2 × 10^9 CFU C. rodentium in a total volume of 100 ul per mouse. T_H17 cells were isolated from colon tissue by Percoll gradient centrifugation (40%/80%) and subjected to flow cytometric sorting at day 10.

RNA-seq

Naive $CD4^+$ T cells from control and *miR-21*$^{-/-}$ mice were differentiated under pathogenic T_H17 (23) differentiation condition. Total RNA was prepared from these cells using Trizol reagent (Invitrogen). RNA-seq libraries were prepared using a TruSeq Stranded Total RNA Library Prep Kit (Illumina). For GFP^+ T_H17 cells sorted from in vivo suspensions, 50,000 cells were resuspended in 700 ul Trizol reagent, total RNA was prepared by miRNeasy Micro Kit (Qiagen), RNA-seq libraries were prepared using SMART-Seq v4 Ultra Low Input RNA Kit (clontech). Sequencing was performed on an Illumina HiSeq X Ten System in a 150 bp/150 bp Paired end mode.

ATAC-seq

ATAC-seq library preparations were performed as described(Buenrostro et al., 2013). In brief, 50,000 cells were washed in cold PBS and lysed. Transposition was performed at 37 °C for 30 min. After purification of the DNA with the

MinElute PCR purification kit (Qiagen), DNA was amplified for 5 cycles. Additional PCR cycles were evaluated by real time PCR. Final product was cleaned by Ampure Beads at a 1.5× ratio. Libraries were sequenced on a HiSeq X Ten System in a 150 bp/150 bp Paired end mode.

Metabolomics

The metabolomics profiling was performed on gas chromatograph-time-of-flight mass spectrometry (GC-TOFMS) as previously described(Chen et al., 2014; Chen et al., 2016). MetaboAnalyst was used to analyze range-scale data and provide PCA and KEGG pathway analysis of metabolites changed (www.metaboanalyst.ca/).

Statistics

Prism software was used for statistical analysis. Differences between groups were compared with an unpaired two-tailed t-test. A P value of less than 0.05 was considered statistically significant.

Acknowledgments

We thank Youcun Qian for kindly sharing with us *C. rodentium* strain DBS100.

Author Contributions

X.Y. and N.S. designed the experiments and wrote the manuscript; X.Y. did most of the experiments; L.W. helped with the mouse experiments; C.Y. and R. Q. helped with the ATAC-seq data analysis; Y.C. helped with cell culture.

Declaration of Interests

The authors declare no competing financial interests.

References

Angelin, A., Gil-de-Gomez, L., Dahiya, S., Jiao, J., Guo, L., Levine, M.H., Wang, Z., Quinn, W.J., 3rd, Kopinski, P.K., Wang, L., et al. (2017). Foxp3 Reprograms T Cell Metabolism to Function in Low-Glucose, High-Lactate Environments. Cell metabolism.

Arsura, M., Wu, M., and Sonenshein, G.E. (1996). TGF beta 1 inhibits NF-kappa B/Rel activity inducing apoptosis of B cells: transcriptional activation of I kappa B alpha. Immunity *5*, 31-40.

Atarashi, K., Tanoue, T., Ando, M., Kamada, N., Nagano, Y., Narushima, S., Suda, W., Imaoka, A., Setoyama, H., Nagamori, T., et al. (2015). Th17 Cell Induction by Adhesion of Microbes to Intestinal Epithelial Cells. Cell *163*, 367-380.

Basu, R., Whitley, S.K., Bhaumik, S., Zindl, C.L., Schoeb, T.R., Benveniste, E.N., Pear, W.S., Hatton, R.D., and Weaver, C.T. (2015). IL-1 signaling modulates activation of STAT transcription factors to antagonize retinoic acid signaling and control the TH17 cell-iTreg cell balance. Nature immunology *16*, 286-295.

Boothby, M., and Rickert, R.C. (2017). Metabolic Regulation of the Immune Humoral Response. Immunity *46*, 743-755.

Buck, M.D., O'Sullivan, D., and Pearce, E.L. (2015). T cell metabolism drives immunity. The Journal of experimental medicine *212*, 1345-1360.

Buenrostro, J.D., Giresi, P.G., Zaba, L.C., Chang, H.Y., and Greenleaf, W.J. (2013). Transposition of native chromatin for fast and sensitive epigenomic profiling of open chromatin, DNA-binding proteins and nucleosome position. Nature methods *10*, 1213-1218.

Ceribelli, M., Hou, Z.E., Kelly, P.N., Huang, D.W., Wright, G., Ganapathi, K., Evbuomwan, M.O., Pittaluga, S., Shaffer, A.L., Marcucci, G., et al. (2016). A Druggable TCF4- and BRD4-Dependent Transcriptional Network Sustains Malignancy in Blastic Plasmacytoid Dendritic Cell Neoplasm. Cancer cell *30*, 764-778.

Chang, C.H., Qiu, J., O'Sullivan, D., Buck, M.D., Noguchi, T., Curtis, J.D., Chen, Q., Gindin, M., Gubin, M.M., van der Windt, G.J., et al. (2015). Metabolic Competition in the Tumor Microenvironment Is a Driver of Cancer Progression. Cell *162*, 1229-1241.

Chang, M., Jin, W., Chang, J.H., Xiao, Y., Brittain, G.C., Yu, J., Zhou, X., Wang, Y.H., Cheng, X., Li, P., et al. (2011). The ubiquitin ligase Peli1 negatively regulates T cell activation and prevents autoimmunity. Nature immunology *12*, 1002-1009.

Chen, W.L., Wang, J.H., Zhao, A.H., Xu, X., Wang, Y.H., Chen, T.L., Li, J.M., Mi, J.Q., Zhu, Y.M., Liu, Y.F., et al. (2014). A distinct glucose metabolism signature of acute myeloid leukemia with prognostic value. Blood *124*, 1645-1654.

Chen, W.L., Wang, Y.Y., Zhao, A., Xia, L., Xie, G., Su, M., Zhao, L., Liu, J., Qu, C., Wei, R., et al. (2016). Enhanced Fructose Utilization Mediated by SLC2A5 Is a Unique Metabolic Feature of Acute Myeloid Leukemia with Therapeutic Potential. Cancer cell *30*, 779-791.

Cho, S., Wu, C.J., Yasuda, T., Cruz, L.O., Khan, A.A., Lin, L.L., Nguyen, D.T., Miller, M., Lee, H.M., Kuo, M.L., et al. (2016). miR-23 approximately 27 approximately 24 clusters control effector T cell differentiation and function. The Journal of experimental medicine *213*, 235-249.

Etchegaray, J.P., and Mostoslavsky, R. (2016). Interplay between Metabolism and Epigenetics: A Nuclear Adaptation to Environmental Changes. Molecular cell *62*, 695-711.

Feng, X., Wang, H., Takata, H., Day, T.J., Willen, J., and Hu, H. (2011). Transcription factor Foxp1

exerts essential cell-intrinsic regulation of the quiescence of naive T cells. Nature immunology *12*, 544-550.
Gagliani, N., Amezcua Vesely, M.C., Iseppon, A., Brockmann, L., Xu, H., Palm, N.W., de Zoete, M.R., Licona-Limon, P., Paiva, R.S., Ching, T., et al. (2015). Th17 cells transdifferentiate into regulatory T cells during resolution of inflammation. Nature *523*, 221-225.
Gaublomme, J.T., Yosef, N., Lee, Y., Gertner, R.S., Yang, L.V., Wu, C., Pandolfi, P.P., Mak, T., Satija, R., Shalek, A.K., et al. (2015). Single-Cell Genomics Unveils Critical Regulators of Th17 Cell Pathogenicity. Cell *163*, 1400-1412.
Ghoreschi, K., Laurence, A., Yang, X.P., Tato, C.M., McGeachy, M.J., Konkel, J.E., Ramos, H.L., Wei, L., Davidson, T.S., Bouladoux, N., et al. (2010). Generation of pathogenic T(H)17 cells in the absence of TGF-beta signalling. Nature *467*, 967-971.
Grumont, R., Lock, P., Mollinari, M., Shannon, F.M., Moore, A., and Gerondakis, S. (2004). The mitogen-induced increase in T cell size involves PKC and NFAT activation of Rel/NF-kappaB-dependent c-myc expression. Immunity *21*, 19-30.
Heise, N., De Silva, N.S., Silva, K., Carette, A., Simonetti, G., Pasparakis, M., and Klein, U. (2014). Germinal center B cell maintenance and differentiation are controlled by distinct NF-kappaB transcription factor subunits. The Journal of experimental medicine *211*, 2103-2118.
Ho, P.C., Bihuniak, J.D., Macintyre, A.N., Staron, M., Liu, X., Amezquita, R., Tsui, Y.C., Cui, G., Micevic, G., Perales, J.C., et al. (2015). Phosphoenolpyruvate Is a Metabolic Checkpoint of Anti-tumor T Cell Responses. Cell *162*, 1217-1228.
Huang da, W., Sherman, B.T., and Lempicki, R.A. (2009). Systematic and integrative analysis of large gene lists using DAVID bioinformatics resources. Nature protocols *4*, 44-57.
Ivanov, II, Atarashi, K., Manel, N., Brodie, E.L., Shima, T., Karaoz, U., Wei, D., Goldfarb, K.C., Santee, C.A., Lynch, S.V., et al. (2009). Induction of intestinal Th17 cells by segmented filamentous bacteria. Cell *139*, 485-498.
Jiang, S., Yan, W., Wang, S.E., and Baltimore, D. (2018). Let-7 Suppresses B Cell Activation through Restricting the Availability of Necessary Nutrients. Cell metabolism.
Kinnaird, A., Zhao, S., Wellen, K.E., and Michelakis, E.D. (2016). Metabolic control of epigenetics in cancer. Nature reviews. Cancer *16*, 694-707.
Littman, D.R., and Rudensky, A.Y. (2010). Th17 and regulatory T cells in mediating and restraining inflammation. Cell *140*, 845-858.
Loeb, G.B., Khan, A.A., Canner, D., Hiatt, J.B., Shendure, J., Darnell, R.B., Leslie, C.S., and Rudensky, A.Y. (2012). Transcriptome-wide miR-155 binding map reveals widespread noncanonical microRNA targeting. Molecular cell *48*, 760-770.
Man, K., and Kallies, A. (2015). Synchronizing transcriptional control of T cell metabolism and function. Nature reviews. Immunology *15*, 574-584.
Mehta, A., and Baltimore, D. (2016). MicroRNAs as regulatory elements in immune system logic. Nature reviews. Immunology *16*, 279-294.
Murugaiyan, G., da Cunha, A.P., Ajay, A.K., Joller, N., Garo, L.P., Kumaradevan, S., Yosef, N., Vaidya, V.S., and Weiner, H.L. (2015). MicroRNA-21 promotes Th17 differentiation and mediates experimental autoimmune encephalomyelitis. The Journal of clinical investigation *125*, 1069-1080.
Najafi-Shoushtari, S.H., Kristo, F., Li, Y., Shioda, T., Cohen, D.E., Gerszten, R.E., and Naar, A.M. (2010). MicroRNA-33 and the SREBP host genes cooperate to control cholesterol homeostasis. Science (New York, N.Y.) *328*, 1566-1569.

Pan, W., Zhu, S., Dai, D., Liu, Z., Li, D., Li, B., Gagliani, N., Zheng, Y., Tang, Y., Weirauch, M.T., et al. (2015). MiR-125a targets effector programs to stabilize Treg-mediated immune homeostasis. Nature communications *6*, 7096.

Philip, M., Fairchild, L., Sun, L., Horste, E.L., Camara, S., Shakiba, M., Scott, A.C., Viale, A., Lauer, P., Merghoub, T., et al. (2017). Chromatin states define tumour-specific T cell dysfunction and reprogramming. Nature *545*, 452-456.

Pollizzi, K.N., and Powell, J.D. (2014). Integrating canonical and metabolic signalling programmes in the regulation of T cell responses. Nature reviews. Immunology *14*, 435-446.

Rayner, K.J., Suarez, Y., Davalos, A., Parathath, S., Fitzgerald, M.L., Tamehiro, N., Fisher, E.A., Moore, K.J., and Fernandez-Hernando, C. (2010). MiR-33 contributes to the regulation of cholesterol homeostasis. Science (New York, N.Y.) *328*, 1570-1573.

Sano, T., Huang, W., Hall, J.A., Yang, Y., Chen, A., Gavzy, S.J., Lee, J.Y., Ziel, J.W., Miraldi, E.R., Domingos, A.I., et al. (2015). An IL-23R/IL-22 Circuit Regulates Epithelial Serum Amyloid A to Promote Local Effector Th17 Responses. Cell *163*, 381-393.

Shi, L.Z., Wang, R., Huang, G., Vogel, P., Neale, G., Green, D.R., and Chi, H. (2011). HIF1alpha-dependent glycolytic pathway orchestrates a metabolic checkpoint for the differentiation of TH17 and Treg cells. The Journal of experimental medicine *208*, 1367-1376.

Stephen, T.L., Rutkowski, M.R., Allegrezza, M.J., Perales-Puchalt, A., Tesone, A.J., Svoronos, N., Nguyen, J.M., Sarmin, F., Borowsky, M.E., Tchou, J., et al. (2014). Transforming growth factor beta-mediated suppression of antitumor T cells requires FoxP1 transcription factor expression. Immunity *41*, 427-439.

Stockinger, B., and Omenetti, S. (2017). The dichotomous nature of T helper 17 cells. Nature reviews. Immunology.

van der Veeken, J., Gonzalez, A.J., Cho, H., Arvey, A., Hemmers, S., Leslie, C.S., and Rudensky, A.Y. (2016). Memory of Inflammation in Regulatory T Cells. Cell *166*, 977-990.

Verbist, K.C., Guy, C.S., Milasta, S., Liedmann, S., Kaminski, M.M., Wang, R., and Green, D.R. (2016). Metabolic maintenance of cell asymmetry following division in activated T lymphocytes. Nature *532*, 389-393.

Wang, R., Dillon, C.P., Shi, L.Z., Milasta, S., Carter, R., Finkelstein, D., McCormick, L.L., Fitzgerald, P., Chi, H., Munger, J., et al. (2011). The transcription factor Myc controls metabolic reprogramming upon T lymphocyte activation. Immunity *35*, 871-882.

Wilhelm, K., Happel, K., Eelen, G., Schoors, S., Oellerich, M.F., Lim, R., Zimmermann, B., Aspalter, I.M., Franco, C.A., Boettger, T., et al. (2016). FOXO1 couples metabolic activity and growth state in the vascular endothelium. Nature *529*, 216-220.

Xu, T., Stewart, K.M., Wang, X., Liu, K., Xie, M., Kyu Ryu, J., Li, K., Ma, T., Wang, H., Ni, L., et al. (2017). Metabolic control of TH17 and induced Treg cell balance by an epigenetic mechanism. Nature *548*, 228-233.

Zhu, H., Shyh-Chang, N., Segre, A.V., Shinoda, G., Shah, S.P., Einhorn, W.S., Takeuchi, A., Engreitz, J.M., Hagan, J.P., Kharas, M.G., et al. (2011). The Lin28/let-7 axis regulates glucose metabolism. Cell *147*, 81-94.

Zhu, S., Pan, W., Song, X., Liu, Y., Shao, X., Tang, Y., Liang, D., He, D., Wang, H., Liu, W., et al. (2012). The microRNA miR-23b suppresses IL-17-associated autoimmune inflammation by targeting TAB2, TAB3 and IKK-alpha. Nature medicine *18*, 1077-1086.

Figure Legends

Figure 1 T_H17 Cells derived in vitro show discrete metabolic states

(A) Western blot analysis of HKII and p-S6 in total protein from $CD4^+$ T cells activated in vitro for indicated time, T_H17 (b) and T_H17 (23) cells differentiated in vitro for 72 h.

(B) Western blot analysis of Foxo1, c-Myc and p-S6 in total protein from T_H17 (b) and T_H17 (23) cells differentiated in vitro for indicated time.

(C) Western blot analysis of HKII and Glut1 in total protein from T_H17 (b) and T_H17 (23) cells differentiated in vitro for indicated time.

(D) Western blot analysis of HKII in total protein from purified GFP^+ T_H17 (b) and T_H17 (23) cells differentiated in vitro for 72 h.

(E) PCA analysis of identified metabolites of T_H17 (b) and T_H17 (23) cells differentiated in vitro for 48 hs by metabolomics.

(F) Metabolomics analysis of T_H17 (b) and T_H17 (23) cells differentiated in vitro for 48 hs, the top differentially observed metabolites are shown in heat map. Data are from one experiment representative of two independent experiments (A, B), >3 independent experiments (C, D).

Figure 2 T_H17 Cells in vivo show discrete metabolic states

(A) Forward scatter plot of T_H17 cells derived in vivo

(B) Side scatter plot of T_H17 cells derived in vivo

(C) Pathway analysis of upregulated genes in CNS T_H17 cells, presented as enrichment for selected pathways.

(D) Heat map of selected genes of interest in T_H17 cell biology.

(E) Heat map of upregulated genes in CNS T_H17 cells related to metabolism pathways.

(F) Heat map of differentially expressed solute carrier family genes.

Figure 3 Chromatin states define T_H17 Cell metabolic reprogramming in vivo

(A) Scatterplots of mean ATAC-seq counts per peak comparing the indicated samples.

(B) Scatterplots of mean ATAC-seq counts per peak comparing the indicated samples.

(C) Principal component analysis (PCA) of peak accessibility in ileum (blue), colon *Citrobacter* (yellow) and CNS (red) T_H17 cells.

(D) ATAC-seq signal profiles across *Ahr*, *c-Maf*, *Foxo1, Pfkfb3* and *Hk3* gene loci.

Figure 4 TGF-β1 signaling remodels T_H17 cell chromatin architecture for metabolic reprogramming

(A) Scatterplots of mean ATAC-seq counts per peak comparing the indicated samples.

(B) Principal component analysis (PCA) of peak accessibility in T_H17 (b) and T_H17 (23) cells.

(C) ATAC-seq signal profiles across *c-Myc*, *c-Rel, c-Maf*, *Ahr* gene loci.

(D) ATAC-seq signal profiles across *Hk2*, *Slc2a1*, *Pgm2* and *Pfkfb2* gene loci.

Figure 5 MiR-21 regulates metabolic reprogramming of T_H17 cells through Peli1-c-Rel axis

(A) ATAC-seq signal profiles across miR-21, miR-23a cluster, miR-210 and miR-125a cluster gene loci.

(B) Heat map of selected genes of interest in T_H17 cell pathogenicity (left) and in glycolytic pathways (right).

(C) Extracellular acidification rate (ECAR) of T_H17 (23) cells differentiated from control and *miR-21*$^{-/-}$ mice for 96 hs assessed by a glycolysis stress test.

(D) Western blot analysis of p-S6 from sorted GFP$^+$ T_H17 cells differentiated under indicated condition.

(E) Comparison of gene list from RNA-seq, Targetscan and CLIP-seq data, showing an overlap of 5 potential miR-21 target genes.

(F) The 3' UTR of Peli1 in activated CD4+ T cells from HITS-CLIP data.

(G) RT-PCR analysis of enriched Peli1 mRNA from Ago2 immunoprecipitated total RNA from in vitro differentiated Control and *miR-21*$^{-/-}$ T_H17(23) cells.

(H) Western blot analysis of Peli1 and c-Rel from sorted GFP$^+$ T_H17 cells differentiated under indicated condition. *$P < 0.05$ (unpaired t-test). Data are from one experiment representative of two independent experiments (C, D, G, H).

Figure 6 MiR-21 regulates T_H17 cells during autoimmunity and mucosal defence

(A) EAE development in CD4-cre and CD4-cre *miR-21*$^{f/f}$ (n=5) mice.

(B) EAE development in Lyz2-cre and Lyz2-cre *miR-21*$^{f/f}$ (n=7) mice.

(C) EAE development in CD11c-cre and CD11c-cre *miR-21*$^{f/f}$ (n=7) mice.

(D) Flow cytometry of IL-17A and IFN-γ secretion by $CD4^+$ T cells isolated from spinal cord of CD4-cre and CD4-cre *miR-21*$^{f/f}$ mice at the peak of disease (n = 4).

(E) Percentage of $IL17A^+$ IFN-$γ^-$, $IL17A^+$ IFN-$γ^+$ and $IL17A^-$ IFN-$γ^+$ cells from spinal cord of CD4-cre and CD4-cre *miR-21*$^{f/f}$ mice as in (D).

(F) Colon length of CD4-cre and CD4-cre *miR-21*$^{f/f}$ mice infected with *Citro Rodentium* for 14 days (n = 4).

(G) Quantification of bacterial burden in colon luminal content at day 14 (n = 4).

(H) Number of total $CD4^+$ T cells of CD4-cre and CD4-cre *miR-21*$^{f/f}$ mice infected with *Citro Rodentium* for 14 days (n = 4).

(I) Number of total T_H1 cells of CD4-cre and CD4-cre *miR-21*$^{f/f}$ mice infected with *Citro Rodentium* for 14 days (n = 4).

(J) Number of total T_H17 cells of CD4-cre and CD4-cre *miR-21*$^{f/f}$ mice infected with *Citro Rodentium* for 14 days (n = 4).

(I) Number of total T_H17*1 cells of CD4-cre and CD4-cre *miR-21*$^{f/f}$ mice infected with *Citro Rodentium* for 14 days (n = 4). Data are from one experiment representative of two independent experiments.

Figure 1

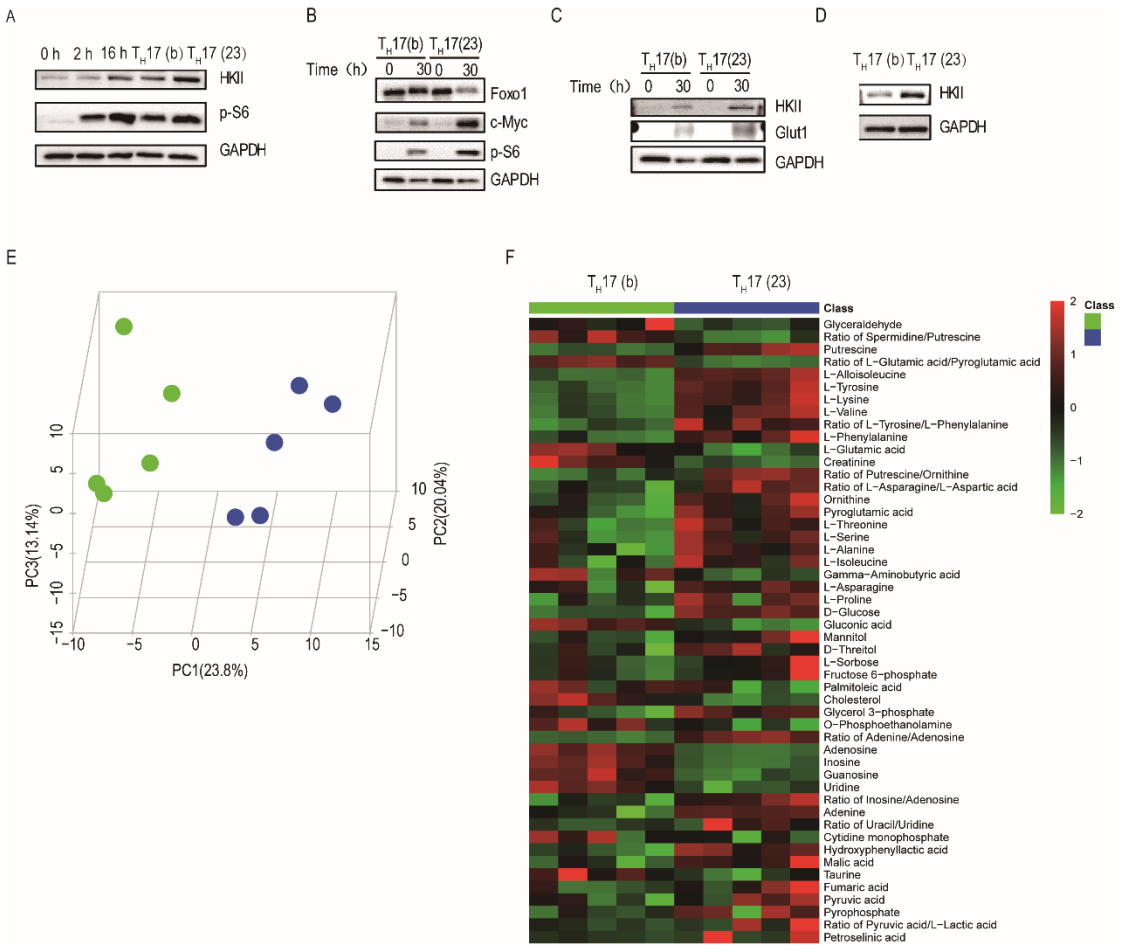
A
0 h
2 h
16 h
T_H17 (b)
T_H17 (23)
HKII
p-S6
GAPDH
B
T_H17(b)
T_H17(23)
Time (h)
0
30
0
30
Foxo1
c-Myc
p-S6
GAPDH
C
T_H17(b)
T_H17(23)
Time (h)
0
30
0
30
HKII
Glut1
GAPDH
D
T_H17 (b)
T_H17 (23)
HKII
GAPDH
E
PC3(13.14%)
PC1(23.8%)
PC2(20.04%)
F
T_H17 (b)
T_H17 (23)
Class
Glyceraldehyde
Ratio of Spermidine/Putrescine
Putrescine
Ratio of L-Glutamic acid/Pyroglutamic acid
L-Alloisoleucine
L-Tyrosine
L-Lysine
L-Valine
Ratio of L-Tyrosine/L-Phenylalanine
L-Phenylalanine
L-Glutamic acid
Creatinine
Ratio of Putrescine/Ornithine
Ratio of L-Asparagine/L-Aspartic acid
Ornithine
Pyroglutamic acid
L-Threonine
L-Serine
L-Alanine
L-Isoleucine
Gamma-Aminobutyric acid
L-Asparagine
L-Proline
D-Glucose
Gluconic acid
Mannitol
D-Threitol
L-Sorbose
Fructose 6-phosphate
Palmitoleic acid
Cholesterol
Glycerol 3-phosphate
O-Phosphoethanolamine
Ratio of Adenine/Adenosine
Adenosine
Inosine
Guanosine
Uridine
Ratio of Inosine/Adenosine
Adenine
Ratio of Uracil/Uridine
Cytidine monophosphate
Hydroxyphenyllactic acid
Malic acid
Taurine
Fumaric acid
Pyruvic acid
Pyrophosphate
Ratio of Pyruvic acid/L-Lactic acid
Petroselinic acid
Class

Figure 2

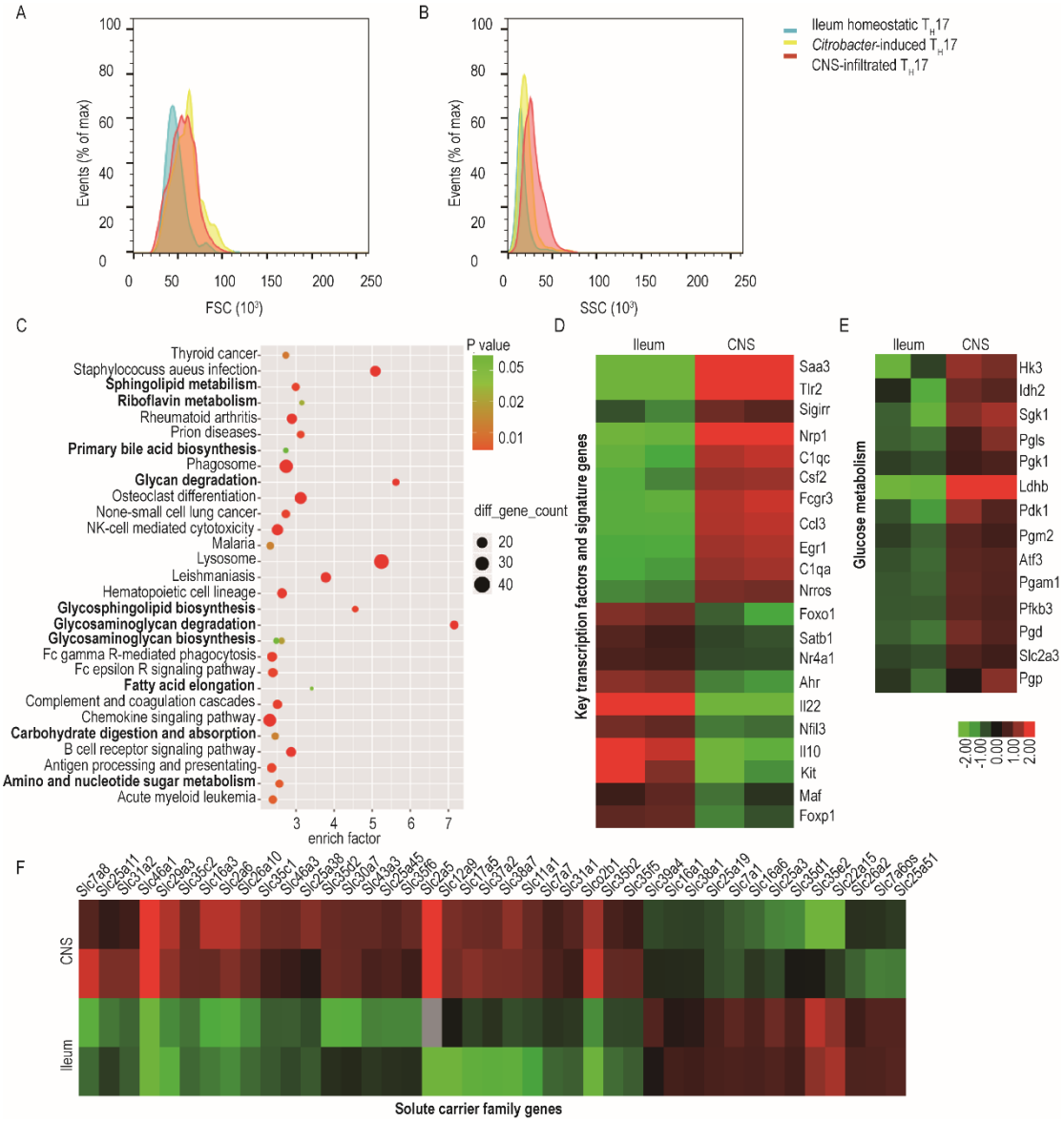
A
B
Events (% of max)
FSC (10³)
SSC (10³)
Ileum homeostatic T_H17
Citrobacter-induced T_H17
CNS-infiltrated T_H17
C
Thyroid cancer
Staphylococuss aueus infection
Sphingolipid metabilism
Riboflavin metabolism
Rheumatoid arthritis
Prion diseases
Primary bile acid biosynthesis
Phagosome
Glycan degradation
Osteoclast differentiation
None-small cell lung cancer
NK-cell mediated cytotoxicity
Malaria
Lysosome
Leishmaniasis
Hematopoietic cell lineage
Glycosphingolipid biosynthesis
Glycosaminoglycan degradation
Glycosaminoglycan biosynthesis
Fc gamma R-mediated phagocytosis
Fc epsilon R signaling pathway
Fatty acid elongation
Complement and coagulation cascades
Chemokine singaling pathway
Carbohydrate digestion and absorption
B cell receptor signaling pathway
Antigen processing and presentating
Amino and nucleotide sugar metabolism
Acute myeloid leukemia
enrich factor
P value
0.05
0.02
0.01
diff_gene_count
20
30
40
D
Ileum
CNS
Key transcription factors and signature genes
Saa3
Tlr2
Sigirr
Nrp1
C1qc
Csf2
Fcgr3
Ccl3
Egr1
C1qa
Nrros
Foxo1
Satb1
Nr4a1
Ahr
Il22
Nfil3
Il10
Kit
Maf
Foxp1
E
Glucose metabolism
Hk3
Idh2
Sgk1
Pgls
Pgk1
Ldhb
Pdk1
Pgm2
Atf3
Pgam1
Pfkb3
Pgd
Slc2a3
Pgp
-2.00
-1.00
0.00
1.00
2.00
F
CNS
Ileum
Solute carrier family genes

Figure 3

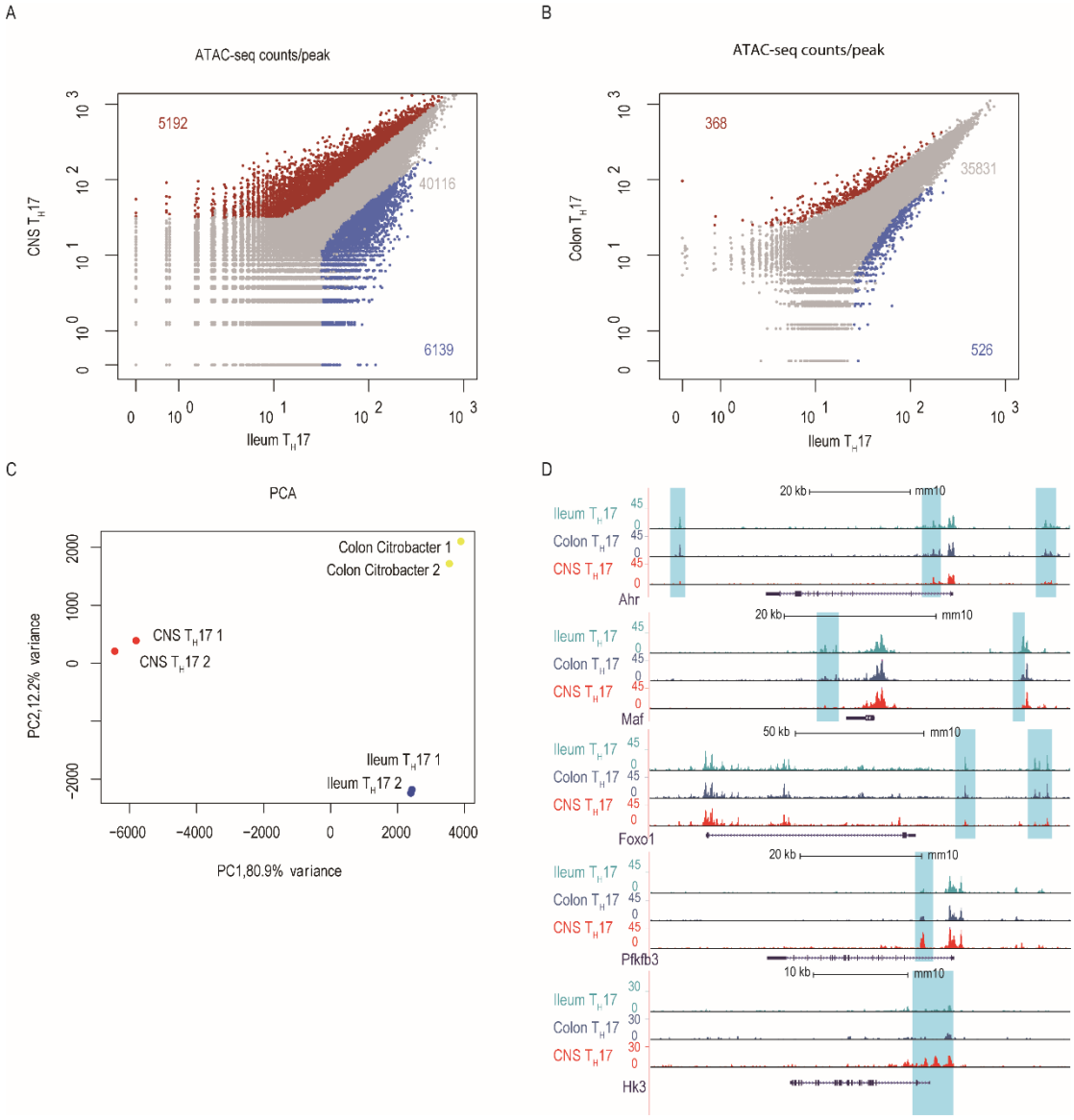
A
ATAC-seq counts/peak
5192
40116
6139
CNS T_H17
Ileum T_H17
B
ATAC-seq counts/peak
368
35831
526
Colon T_H17
Ileum T_H17
C
PCA
Colon Citrobacter 1
Colon Citrobacter 2
CNS T_H17 1
CNS T_H17 2
Ileum T_H17 1
Ileum T_H17 2
PC2,12.2% variance
PC1,80.9% variance
D
Ileum T_H17
Colon T_H17
CNS T_H17
Ahr
Maf
Foxo1
Pfkfb3
Hk3
20 kb
50 kb
10 kb
mm10

Figure 4

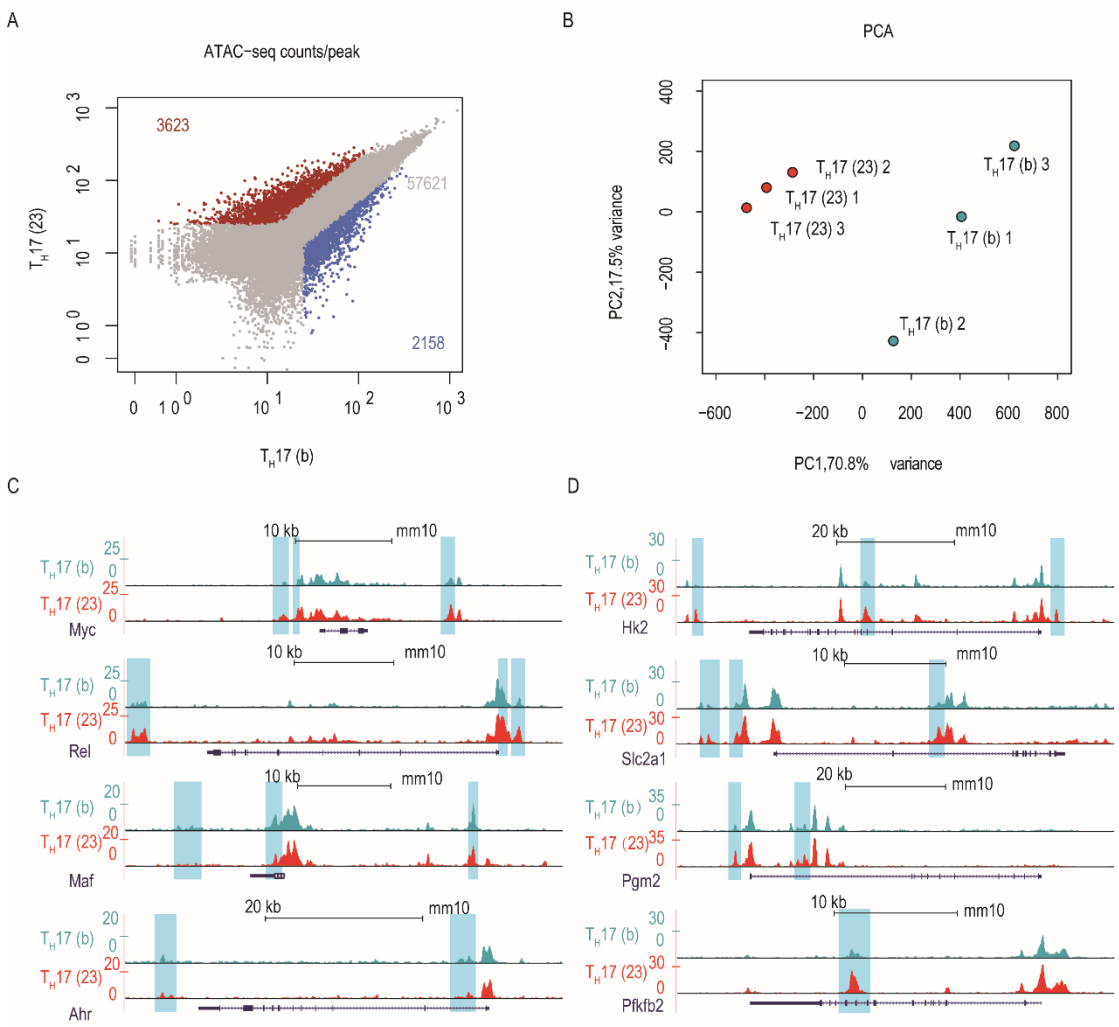
A
ATAC−seq counts/peak
3623
57621
2158
T_H17 (23)
T_H17 (b)
B
PCA
T_H17 (23) 2
T_H17 (23) 1
T_H17 (23) 3
T_H17 (b) 3
T_H17 (b) 1
T_H17 (b) 2
PC2,17.5% variance
PC1,70.8% variance
C
D
10 kb
20 kb
mm10
T_H17 (b)
T_H17 (23)
Myc
Rel
Maf
Ahr
Hk2
Slc2a1
Pgm2
Pfkfb2

Figure 5

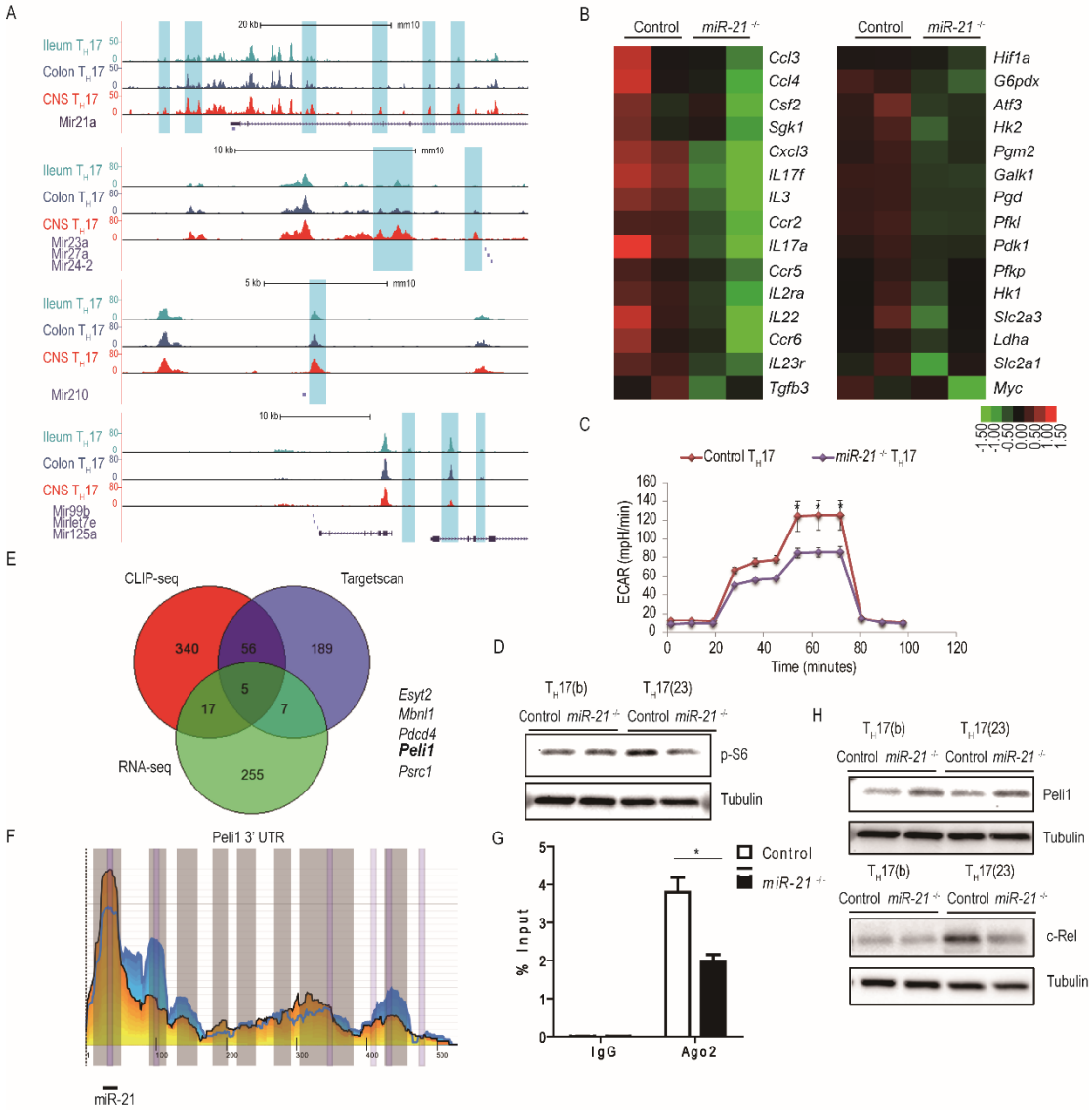
A
Ileum TH17
Colon TH17
CNS TH17
Mir21a
Mir23a
Mir27a
Mir24-2
Mir210
Mir99b
Mir let7e
Mir125a
B
Control
miR-21 -/-
Ccl3
Ccl4
Csf2
Sgk1
Cxcl3
IL17f
IL3
Ccr2
IL17a
Ccr5
IL2ra
IL22
Ccr6
IL23r
Tgfb3
Hif1a
G6pdx
Atf3
Hk2
Pgm2
Galk1
Pgd
Pfkl
Pdk1
Pfkp
Hk1
Slc2a3
Ldha
Slc2a1
Myc
C
Control TH17
miR-21 -/- TH17
ECAR (mpH/min)
Time (minutes)
D
TH17(b)
TH17(23)
p-S6
Tubulin
E
CLIP-seq
Targetscan
RNA-seq
340
56
189
5
17
7
255
Esyt2
Mbnl1
Pdcd4
Peli1
Psrc1
F
Peli1 3' UTR
miR-21
G
% Input
IgG
Ago2
H
Peli1
c-Rel
Tubulin

Figure 6

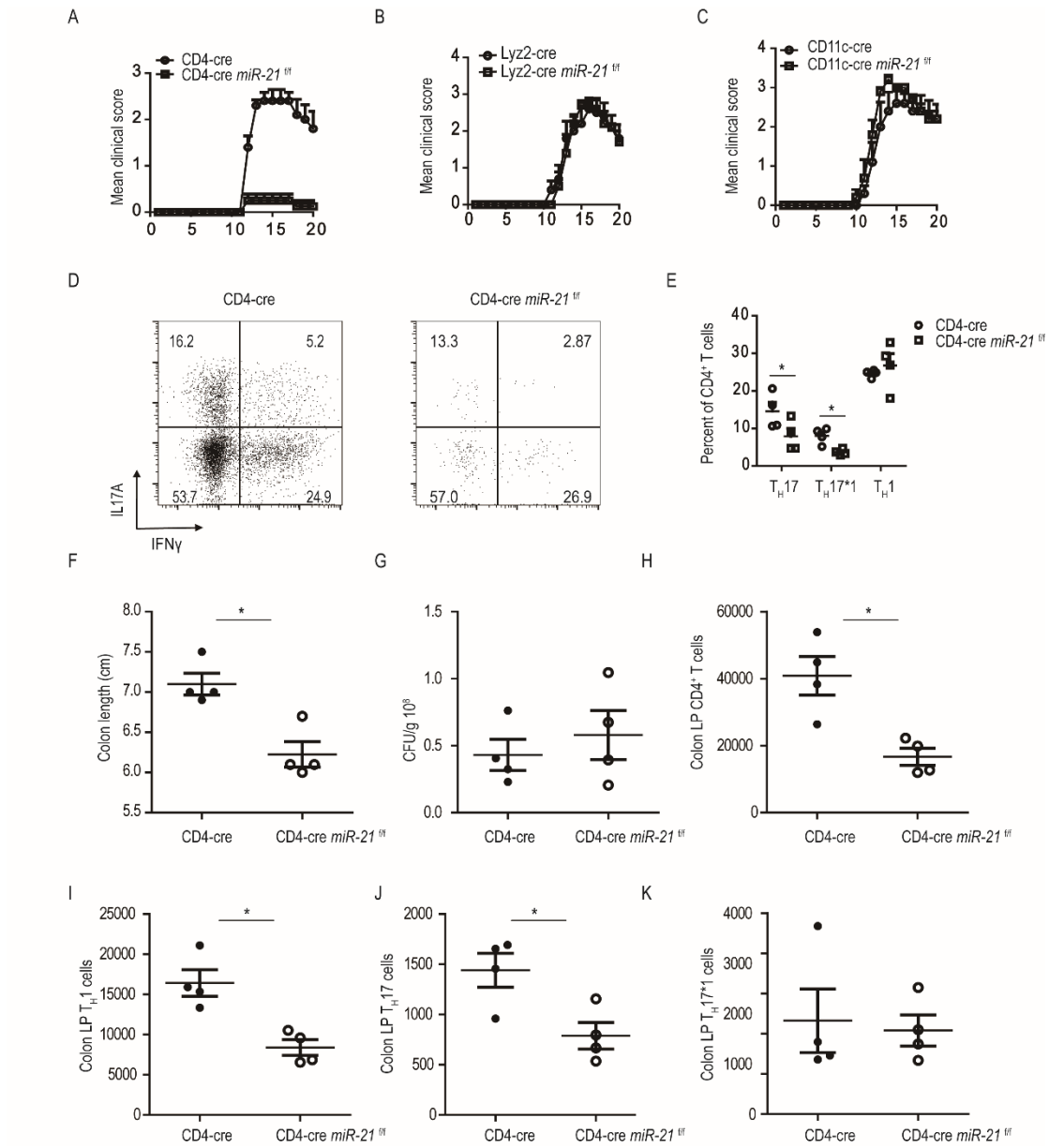
A
CD4-cre
CD4-cre miR-21 f/f
Mean clinical score
B
Lyz2-cre
Lyz2-cre miR-21 f/f
C
CD11c-cre
CD11c-cre miR-21 f/f
D
CD4-cre
CD4-cre miR-21 f/f
16.2
5.2
53.7
24.9
13.3
2.87
57.0
26.9
IL17A
IFNγ
E
Percent of CD4+ T cells
TH17
TH17*1
TH1
F
Colon length (cm)
G
CFU/g 10³
H
Colon LP CD4+ T cells
I
Colon LP TH1 cells
J
Colon LP TH17 cells
K
Colon LP TH17*1 cells